ISSN: 0001-5113 AADRAY	ACTA ADRIAT., 59 (1): 17 - 34, 2018	ORIGINAL SCIENTIFIC PAPER

Monitoring the eutrophication using Landsat 8 in the Boka Kotorska Bay

Blažo ĐUROVIĆ[1], Igor ĐUROVIĆ[1], Aleksandar JOKSIMOVIĆ[2], Vladimir CRNOJEVIĆ[3], Slobodan ĐUKANOVIĆ[1] and Branka PESTORIĆ[2]

[1] University of Montenegro, Faculty of Electrical Engineering, Džordža Vašingtona bb, 81000 Podgorica, Montenegro

[2] University of Montenegro, Institute of Marine Biology, P. O. Box 69, 85330 Kotor, Montenegro

[3] BioSense Institute, dr. Zorana Djindjica 1, 21000 Novi Sad, Serbia

Corresponding author, e-mail: blazodj@ac.me

This study proposes a methodology for monitoring concentrations of chlorophyll a (Chl-a) and the state of eutrophics in small bays or in the immediate vicinity of the coast. This kind of monitoring is of interest since such areas have not been addressed well using the usual satellite methods (such as MODIS) due to inadequate spatial resolution. We present an estimation approach for Chl-a concentration based on Landsat 8 (L8) satellite images using the ground truth (GT) data for the day of overflight. Additionally, two classifiers (daily and yearly) of the state of eutrophication, that use the Chl-a estimated values, are presented. The accuracy of the proposed method is evaluated using the leave-one-out cross validation, and it is within limits theoretically expected of an L8-based approach. The results from the classifiers are compared with the GT data and it is shown that daily classifier is able to classify the area of interest with an incidence of false positives less than 2%.

Key words: Remote sensing, chlorophyll *a*, eutrophication, Landsat 8

INTRODUCTION

Eutrophication is characterized by excessive primary production due to increased availability of one or more limiting growth factors needed for photosynthesis (SCHINDLER, 2006). Eutrophication, which can be natural or more commonly of anthropogenic origin, has recently become a significant problem in coastal areas, especially in enclosed bays (VOLLENWEIDER *et al.,* 1992; DEGOBBIS *et al.,* 2000; TETT *et al.,* 2003).

Most eutrophication assessment methods recognize that the immediate biological response is increased primary production reflected as increased chlorophyll *a* (Chl-*a*) and/or macroalgal abundance (BRICKER *et al.,* 2007; OSPAR, 2008; NIXON, 2009; NINČEVIĆ-GLADAN *et al.,* 2015). Determination of Chl-*a* as the main photosynthetic pigment is the most common method for estimating the crop of primary producers in the marine environment (STRICKLAND & PARSONS, 1972). Large increase in the Chl-*a* concentration (bloom) may cause impacts such as the displacement of indigenous taxa, habitat alteration and oxygen depletion. Some phytoplankton taxa are toxic; their blooms cause illness and death

in humans, fish, seabirds, marine mammals, and other oceanic life, often because of toxin transfer through the food web (ANDERSON *et al.,* 2010). Therefore, obtaining the information about potential eutrophication and high concentrations of Chl-*a* would enable timely response and planning of additional sampling parameters and laboratory analyses. Considering that 19 shellfish and fish farms are located in Boka Kotorska Bay (STATISTICAL OFFICE OF MONTENEGRO, 2014) and that the bivalves are filter feeders, any filtration of water of lower quality could lead to bioaccumulation of harmful substances in shell tissue and thus undesirable consequences for end users, i.e. consumers and the general population. This makes regular monitoring of water quality an even greater priority.

Seawater monitoring campaigns are rather expensive since they require costly equipment and materials, transportation, trained technicians and taking samples in scheduled intervals. However, technological progress has provided the means for overcoming these issues.

Satellites constantly survey the entire surface of the Earth. The data of numerous satellites can be acquired free of charge. Today, oceans are monitored on daily basis by the MODIS (NASA, 2015a) sensor on Aqua (2002) and Terra (1999) satellites (NASA, 2015b) specifically designed for use in ocean color (OC) studies. They offer daily maps of Chl-*a* concentrations (SAVTCHENKO *et al.,* 2004). Unfortunately, MODIS has a relatively low spatial resolution (1 km) (the physical size of a pixel on a satellite image) for our purposes. This is because the purpose of this work is to perform remote sensing of small bays such as Boka Kotorska Bay, which itself is approx. 5km wide at its widest and considerably narrower otherwise (see "Study Area" section and Figures 2-3 for more details). Hence, on a MODIS image, the bay is represented by a small number of pixels, of which quite a few are contaminated by land areas, which is far too few to properly resolve all the features of the bay.

Other satellites were also considered for remote sensing of water quality and ecosystem monitoring as shown by (OLMANSON, *et al.,* 2001; HELLWEGER *et al.,* 2004; OLET, 2010; NEUKERMANS *et al.,* 2009; VANHELLEMONT & RUDDICK, 2014). Significant attention has been paid to the problem of monitoring various water quality parameters in lakes (DANBARA 2014; OLET, 2010; OLMANSON *et al.,* 2001; BARRETT & FRAZIER, 2016) (MCCULLOUGH *et al.,* 2012; ALLAN *et al.,* 2011) some of which were quite advanced in their methodology and used Landsat 8 (CONCHA & SCHOTT, 2016). There have been studies done in the Adriatic (MÉLIN *et al.,* 2011) that used remote sensing, and even used Landsat 8 satellite, but they tend to be done on the open Adriatic, for example in (BRANDO *et al.,* 2015) where remote sensing was used for Turbidity and Sea Surface Temperature mapping. On the other hand, the use of remote sensing to monitor the seawater quality along the coasts and in bays where MODIS cannot be used has received considerably less attention. Probably the closest was (FOCARDI *et al.,* 2009) where the Landsat 7 data was used to create false color images of the bay to provide details, but MODIS was used for Chl-*a* concentrations since the bay was large enough to be resolved by it.

Landsat 8 (L8) (IRONS *et al.,* 2012) is the newest satellite of the Landsat family of land observing satellites operated by United States Geological Survey (USGS) whose data is available free of charge (EROS, 2015). L8's sensor, Optical Land Imager, has a medium spatial resolution (30m) and high radiometric precision. These characteristics are important because, as mentioned previously, the study area is a relatively narrow bay, therefore the pixels of the satellite image need to be small enough to resolve the bay's features. High radiometric precision is important because the variance of light reflected from the sea surface tends to be low, compared to the land, so high precision is needed to detect subtle changes in reflected light caused by processes going on beneath the surface. It also has several bands in visible spectrum that could be used for OC studies. A study (GERACE *et al.,* 2013) has demonstrated L8's great potential for monitoring of coastal water based on the simulated data.

Parts of this research dealing with the Chl-*a* estimation have already been presented in very broad strokes in (KOSTIANOY *et al.,* 2016.) as part of a general overview on remote sensing of the study area. In this paper, the methodology

referenced above is described in more detail, and more importantly, the idea of monitoring eutrophication in the bay is introduced.

In this paper, we propose methods to use L8 satellite images for water quality monitoring, that is detection of areas undergoing eutrophication. For that purpose, we use the ground truth (GT) Chl-*a* sampling, performed by University of Montenegro, Institute of Marine Biology of Kotor (IMBK), to create models that predict Chl-*a* and trophic state from the L8 sensed sea surface reflectances (L8 SSR). The final products are maps showing the most likely areas that are undergoing eutrophication on both daily and yearly level.

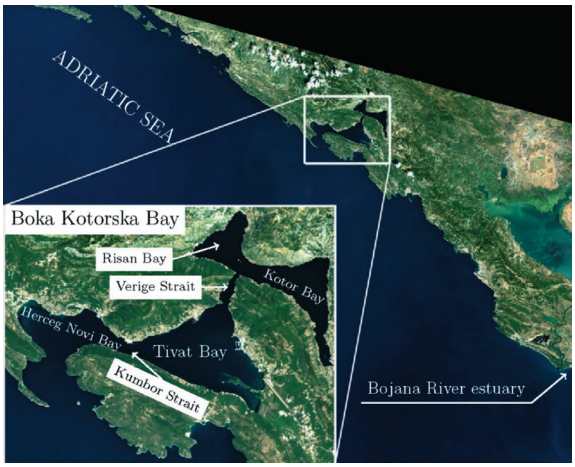

Fig 1 Boka Kotorska Bay and south-eastern Adriatic

Study Area

Boka Kotorska Bay is the largest bay in the south Adriatic Sea and is located on its south-eastern coast (Figure 1). The total surface area is 87.3 km^2, total coast length is 105.7 km and the maximum depth is 60 m (STJEPČEVIĆ & ŽUNJIĆ, 1964). The bay area is split between four bays: Risan, Kotor, Tivat and Herceg-Novi Bays (Figure 1). In this paper bays are often grouped into the inner bay section (Risan and Kotor Bays)

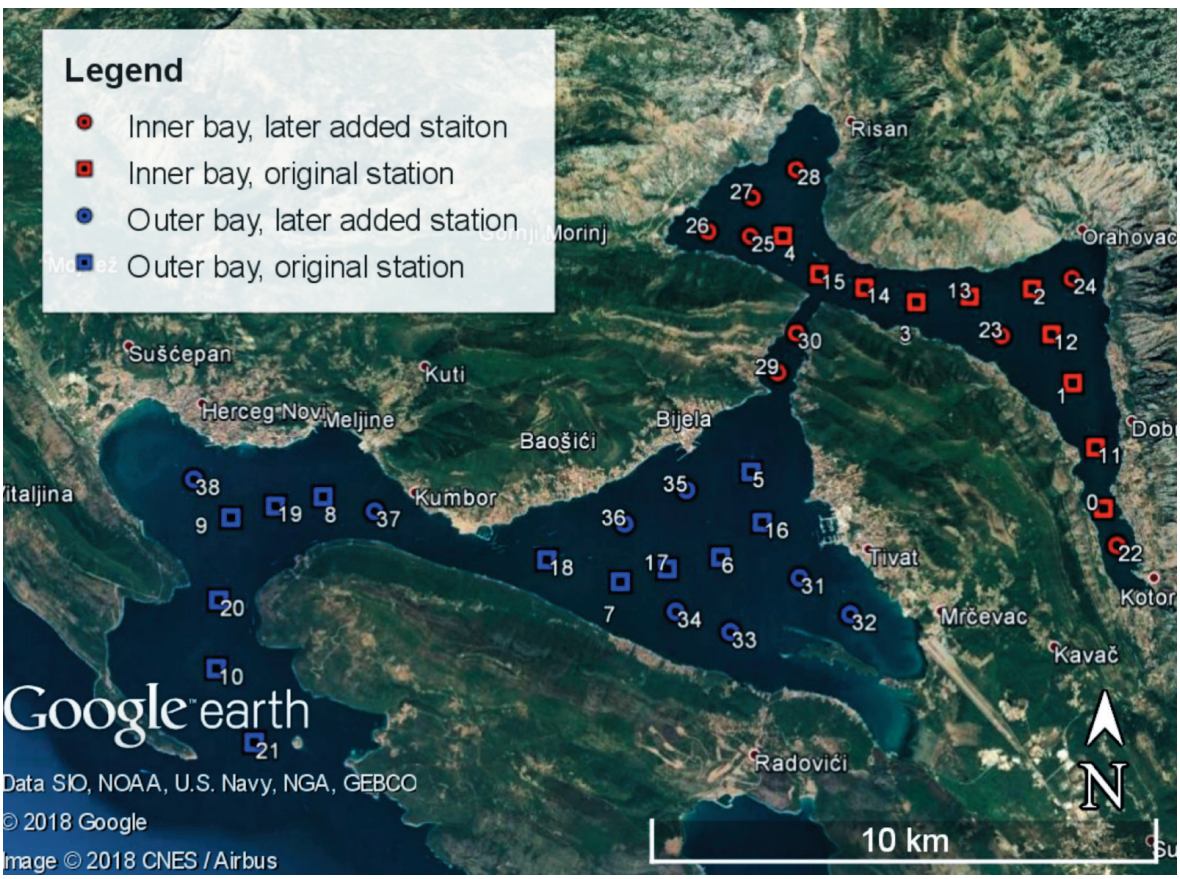

Fig 2 Sampling station locations in the Boka Kotorska bay. Stations in the inner part shown in red while those in the outer are in blue.

and the outer bay section (Tivat and Herceg-Novi Bays). The inner section is characterized by underground rivers and underwater springs, which influence the physical-chemical parameters (LEPETIĆ, 1965; MILANOVIĆ, 2007; BELLAFIORE *et al.,* 2011). More importantly, as shown in the "Results" section, the Chl-*a* concentrations in the inner bay tend to be significantly larger than in the outer one.

The previous studies have shown that the annual rainfall pattern has a significant influence on nutrient-loading seasonality in Boka Kotorska Bay (KRIVOKAPIĆ *et al.,* 2009), since the bay is surrounded by high (above 1500 m) and steep limestone mountains of the Dinaric Alps, which have one of the highest levels of precipitation (4584 mm per year) in Europe (MAGAŠ, 2002).

MATERIAL AND METHODS

Ground truth campaign

Chl-*a* concentrations were measured by taking water samples, from predetermined locations scattered all over the bay, during L8 overflights (every 16 days) when weather conditions were favorable. Fourteen sampling cruises were performed during 2015, namely on 15th and 31st of March, 16th of April, 18th of May, 3rd and 19th of June, 5th and 21st of July, 6th of August, 7th and 23rd of September, 10th of November and 12th and 28th of December.

The locations of sampling stations are shown in Fig. 2. Red markers are used for stations in the inner bay area (0-4, 11-15 and 22-30), whereas the blue ones are for the outer bay (5-10, 16-21, 31-38). The initial eleven samplings were performed at only 22 stations (labeled as 0-21 with square markers), whereas only the cruises in November and December started collecting water samples from all 39 stations (added stations marked with circular markers). In total, 301 measurements of Chl-*a* were performed.

Samples were collected from sea surface using 5L Niskin bottles (HydroBios, Germany). Water samples (2L) for Chl-*a* measurement were pre-filtered through a 330μm mesh net to remove large zooplankton. After filtration through the Whatman GF/F filters, extraction was performed in 90% acetone using ultrasonic stick (Cole Parmer) and Chl-*a* was calculated from the absorbance values (JEFFREY *et al.,* 1997) measured using Analytik-Jena SPECORD 250/ plus UV/VIS spectrophotometer. According to (WRIGHT et al. 2005), this method of measurement has an error in range of 1-3%, which is assumed acceptable for our purpose.

L8 sea surface reflectance

As previously explained, the L8 satellite data is used in this study instead of data from other satellites due to its spatial resolution (30m with respect to 250-1000m in MODIS (NASA, 2015b)), which is necessary to resolve inlets and bays in our area of interest. However, the downside of increased spatial resolution is low temporal resolution since L8 has a revisit time of 16 days, which is quite low compared to daily snapshots provided by the Aqua/Terra pair of satellites carrying MODIS.

The SSR is computed by correcting the Top of the Atmosphere (TOA) reflectance for the effects of gaseous absorption (O_3 and H_2O), Rayleigh reflectance and then for specular reflection (glint) from the sea surface. The following is the expression based on (VERMOTE, et al., 2006) (KOTCHENOVA *et al.* 2006) used to compute the SSR:

$$\rho_w(b) = \frac{\rho_{TOA}(b)/t_g(b) - \rho_r(b)}{t_r(b)}, \qquad (1)$$

where $\rho_w(b)$, $\rho_{TOA}(b)$ and $\rho_r(b)$ are the sea surface, TOA and Rayleigh reflectance, respectively, *b* refers to the L8 band and $t_g(b)$ and $t_r(b)$ are the gaseous and Rayleigh transmittances, respectively. Due to difficulty with designing a proper aerosol correction algorithm, SSR was not corrected for the presence of aerosols. For the Sun glint removal, we used the method of Hedlay *et al*. (HEDLEY *et al*., 2005; KAY *et al*., 2009). A more detailed description of the entire process is povided in the appendix.

Chl-a estimation

To determine potentially eutrophicated areas, a map of Chl-*a* concentrations is needed, which can be obtained from L8 SSR gained by performing the atmospheric and glint correction as described previously.

A map of Chl-*a* concentrations can only be obtained from L8 RSS for days when L8 overflies the area of interest, and skies are cloudless. On such days, GT values were collected from sample points shown in Figure 2. Using this daily dataset, containing only the GT Chl-*a* values for that day, and L8 SSR at the station where GT Chl-*a* was measured, a relation between GT Chl-*a* and L8 SSR for that day is determined by fitting (modeling) six candidate relations (based on OBPG's Chl-*a* retrieval algorithm (O'REILLY *et al*., 2000) using regression and picking the best.

The first three are obtained by polynomial interpolation using a polynomial function $f(x)$

$$\log_{10}(C_a) = f_n(\log_{10}(R_{L8})), \quad (2)$$

$$f_n(x) = a_0 + \sum_{i=1}^{n} a_i \log_{10}(x)^i \quad (3)$$

where C_a is Chl-*a*, $n \in [1,3]$ is the polynomial order of the function, R_{L8} is the L8 band ratio and a_i are the coefficients that are determined by linear regression. The other three relations are obtained by non-linear interpolation of $g(x)$

$$C_a = g_n(\log_{10}(R_{L8})), \quad (4)$$

$$g_n(x) = 10^{f_n(x)}. \quad (5)$$

While both (2) and (4) are essentially the same, they are processed (fitted) differently, with (2) being fitted to $\log_{10}(C_a)$ and $\log_{10}(R_{L8})$ using linear interpolation while (4) is fitted to C_a and $\log_{10}(R_{L8})$ using non-linear interpolation, which in practice produces different coefficients a_i . All six candidates have been fitted using fit function in MATLAB.

L8 band ratio is:

$$R_{L8} = \max(R_G^{CA}, R_G^B), \quad (6)$$

where *CA*, *B* and *G* denote L8 Coastal Aerosol, Blue and Green bands (Bands 1-3) and represents the reflectance ratio $\rho(A)/\rho(B)$ of bands *A* and *B*. This choice of bands for the band ratio is meant to mimic the OBPG's Chl-*a* retrieval algorithm's band ratio (O'REILLY, *et al.,* 2000) for MODIS satellite max $(R_{547}^{443}, R_{547}^{490})$. While the L8 bands are wider but they do cover the same wavelengths MODIS bands use. Table 1 shows a comparison of MODIS and L8 bands in question.

Table 1 Comparison between bands involved in Chl-a sensing of L8 and MODIS

Landsat 8		**MODIS**	
Band	**Wavelength (nm)**	**Wavelength (nm)**	**Band**
Band 1 (Coastal Aerosol)	430-450	438-448	Band 9
Band 2 (Blue)	450-515	483-493	Band 10
Band 3 (Green)	525-600	546-556	Band 12

Out of six candidate functions, one is chosen as follows. First, all non-decreasing functions in the observed range of R_{L8} for the day are removed from consideration. Then the function with the smallest root mean square error (RMSE) between the GT Chl-*a* and the estimated Chl-*a* is chosen. The selected function is considered the retrieval algorithm for that day and used to retrieve Chl-*a* concentrations for the entire bay on a pixel-by-pixel basis.

Detecting eutrophication

Two eutrophication classifiers were designed. The first one is a daily classifier that uses a map of Chl-*a* concentrations estimated from L8 data (see previous section), to classify the pixels into classes based on confidence in presence of eutrophication. Seas where the Chl-*a* concentration is over 2.21 mg m^{-3} can be considered to be under the influence of eutrophication (SIMBOURA *et al.*, 2005). For the sake of brevity, the units of measurement for the Chl-*a* concentrations (mg m-3) are omitted hereafter.

Due to the presence of Chl-*a* estimation error, estimated Chl-*a* above threshold 2.21 cannot be surely declared as subject to eutrophication and vice versa. However, the GT Chl-*a* values give us the ability to analyze the statistical properties of the estimation error. Therefore, in order to avoid false positives and still be able to assess potentially eutrophicated areas, all sea pixels of the bay will be classified into 4 classes based on how confident we are in eutrophication, as follows:

• low chance of eutrophication:

$$C_a^{est} \le 2.21 - P_e(87.5);$$

• possible eutrophication:

$$2.21 - P_e(87.5) < C_a^{est} \le 2.21 - P_e(12.5);$$

• probable eutrophication

$$(p \approx 87.5\%): 2.21 - P_e(12.5) < C_a^{est} \le 2.21 + \max(|e|);$$

• certain eutrophication:

$$C_a^{est} > 2.21 + \max(|e|).$$

Here, n is the n-th percentile of the set of estimation errors e. The estimation error is $e = C_a^{GT} - C_a^{est}$, where *GT* and *est* denote the GT and estimated Chl-*a* values, respectively.

The last two classes are considered positive findings of eutrophication with just different probabilities of validity. Detecting possible eutrophication can be considered as alarming, requiring further analysis. The low chance class should rarely be applied on areas where eutrophication is actually present. This classification scheme is applied per pixel on the maps of estimated Chl-*a*.

The second classifier performs a yearly classification based on Chl-*a* concentrations from multiple dates and seasons. According to (SMODLAKA, 1986), ratio of maximum summer to average Chl-*a* can be used as an indicator of eutrophication, where the locations with ratio greater than five can be considered to have been affected by eutrophication during the year. Maximum summer concentration was used because in the area of study (Northern Adriatic), the summer is the most productive period of the year with the most nutrients available and highest Chl-*a*. On the other hand, it has been shown ("Results" section and (KRIVOKAPIĆ *et al.*, 2011)) that this is not the case for Boka Kotorska Bay. Its most productive (highest Chl-*a*) period of the year is the non-summer portion of the year with heaviest rainfall. Therefore, ratio of maximum non-summer (also referred to as "winter") to average Chl-*a* is used.

For the purposes of this study and considering the expeditions performed, five cruises are considered as having occurred during non-summer/"winter". The cruises in question took place on 15th and 31st of March, 16th of April, and 12th and 28th of December. The November cruise would have also been included but atmospheric conditions on that day were not favorable for remote sensing.

This ratio is also computed in per pixel manner based on the estimated Chl-*a* concentrations. The product of this classifier is a map of these ratios which will be referred to as yearly eutrophication classification indicator or yearly eutrophication indicator with a note that values over five indicate pixels likely affected by eutrophication.

Leave-one-out validation

Since there is no alternative dataset to validate the estimation and classification against, leave-one-out (LOO) (DEVROYE, 2013) methodology was used for validation. To compute the LOO estimation error for a specific data point (GT Chl-*a* concentration for certain station and day), the daily GT dataset it belongs to is taken and the data point is removed from it. This partial dataset is then used to train the retrieval algorithm (as shown in the "Chl-*a* estimation" section) which is used to estimate the Chl-*a* concentration for that day and station. The LOO error is the difference between the actual GT concentration and the concentration estimated using a retrieval algorithm trained on the partial dataset. Therefore, the specific LOO error $e_{LOO}(d,l)$ is

$$e_{LOO}(d,l) = C_{aGT}(d,l) - c_d^l(R_{L8}(d,l)) \quad (7)$$

where $C_{aGT}(d,l)$ is the GT Chl-*a* concentration for day d and station l, c_d^l is the retrieval function trained on the dataset for day d out of which station l has been left out and $R_{L8}(d,l)$ is the L8 band ratio for station l on day d.

Results

GT campaign

Figure 3 shows the colormap of the concentrations measured by the GT campaign. The x-axis represents the stations, here denoted with their corresponding station ids given in Figure 2. The y-axis contains the dates on which cruises were performed. The color bar shows the colors associated with the values in mg m^{-3}. Dark blue negative values represent the stations not surveyed. They are most notable in the "upper right" section of the figure since stations 22-30 were only surveyed during the last three cruises.

Figure 4 shows the mean Chl-*a* values for each cruise. The mean Chl-*a* concentrations are shown separately for the inner (blue line with circle marks) and outer (red line with square marks) bay area. The vertical bars show standard deviation of the samples, i.e.

$$std(d) = \sqrt{\frac{1}{N-1}\sum_l \left|C_{GT}(d,l) - \mathrm{C}_{mean}(d)\right|^2} \qquad (8)$$

where $\mathrm{C}_{mean}(d)$ is the mean Chl-*a* concentration:

$$\mathrm{C}_{mean}(d) = \frac{1}{N}\sum_l C_{GT}(d,l) \qquad (9)$$

and N is the number of stations surveyed.

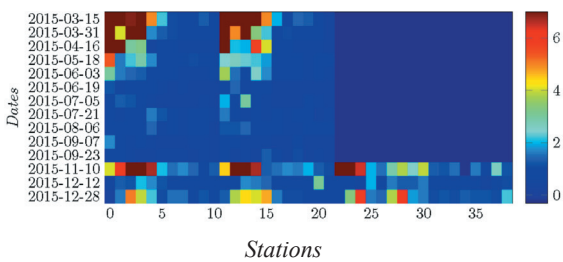

Fig. 3 Chlorophyll a concentrations measured by the Ground Truth campaign in mg m-3. Stations are represented by their id numbers. For details check Figure 2.

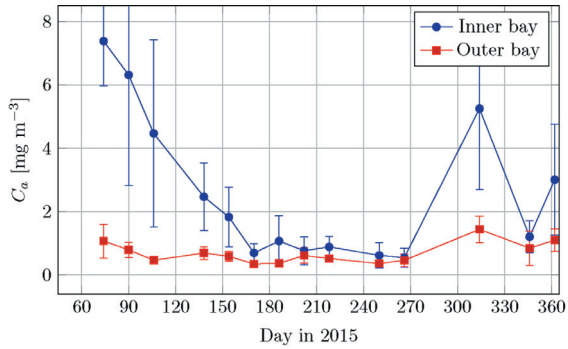

Fig. 4 Average Chlorophyll a concentration measured during each cruise of the Ground Truth campaign, for the inner (blue) and outer (red) bay areas. Dates (horizontal axis) are presented as day in year (1st of January is 1, 1st of February is 32 etc.).

Figures 3 and 4 show that the Chl-*a* concentration in the inner parts of the bay tends to be considerably higher than in the outer section, especially during the rainy spring and autumn months. In general, the concentration in the outer part of the bay is less than 1 mg m^{-3}, whereas in the inner part of the bay the concentration ranges from 0.33 mg m^{-3} to 11 mg m^{-3}. Median inner bay concentration is 1.6 mg m^{-3}, whereas for the outer part it is 0.54 mg m^{-3}.

On October 26th, 2016, in an effort to estimate actual systematic error of the GT campaign (in theory it should be 1-3% (WRIGHT et al. 2005)), on 8 stations, two water samples per station were taken along the coast of the bay. The absolute difference between the two samples ranged from 0.007 to 0.547 with an average of 0.221. Relative difference, $2(C_1 - C_2)/(C_1 + C_2)$, where C_1 and C_2 are the concentrations, ranging from 0.16% to 23.07% with an average of 9.61%.

Chl-*a* estimation

During our campaign, five out of 19 possible overflight days between March 15th and December 28th, or 26%, were unsuitable for satellite remote sensing. During the GT campaign, 301 measurements were made, but due to the clouds, shadows cast by clouds and other conditions, 57 (or 19%) of those measurements could not be matched with L8.

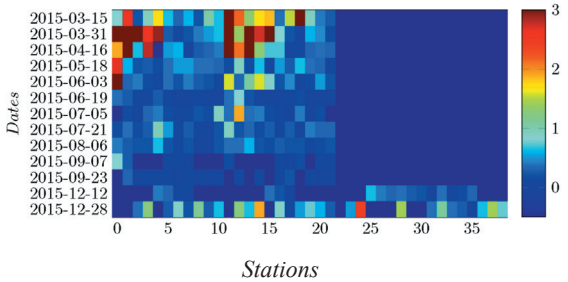

Fig. 5 Absolute Chlorophyll a estimation error (in mg m-3) according to the leave-one-out validation methodology. Stations are represented by their id numbers. For details, check Figure 2.

Figure 5 shows the colormap of the absolute estimation errors per LOO methodology, which has been explained in "Leave-one-out validation" section. Estimation has not been performed for the cruise in November due to contamination of atmosphere with water vapor which made atmospheric correction unreliable.

Dark blue (less than 0) points indicate that the estimated Chl-*a* concentration could not have been matched with the GT concentration because either sample has not been taken for that station on that day, or the station was obscured by clouds or cloud shadows, preventing estimation. The second case is the cause of the majority of "missing" data for the cruises from September on.

Mean and median of the absolute LOO error is 0.63 mg m^{-3} and 0.266 mg m^{-3} respectively, whereas the standard deviation is 0.93 mg m^{-3}. Mean and median of the actual estimation error (not LOO) is 0.4779 mg m^{-3} and 0.234 mg m^{-3} respectively.

Figure 6 shows the Chl-*a* estimation normalized RMSE (NRMSE) for each of the observation days separately. The RMSE was normalized by the range of Chl-*a* concentrations measured by GT on that day. Therefore, the NRMSE is defined as

$$NRMSE = \frac{\sqrt{\frac{1}{N}\sum_{n=1}^{N}\left[C_a^{GT}(n) - C_a^{est}(n)\right]^2}}{\max\{C_a^{GT}(n)\} - \min\{C_a^{GT}(n)\}}, \quad (10)$$

where $C_a^{GT}(n)$ is the *n*th GT Chl-*a* sample, $C_a^{est}(n)$ is the estimated Chl-*a* for the station where the *n*th sample has been retrieved. *N* represents the total number of samples measured and matched with L8 data. Cases where either the GT measurement or Chl-*a* estimation has not been performed were not considered. The average NRMSE for all days is 12.67%, while the NRMSE for all samples taken as whole is 6.11%.

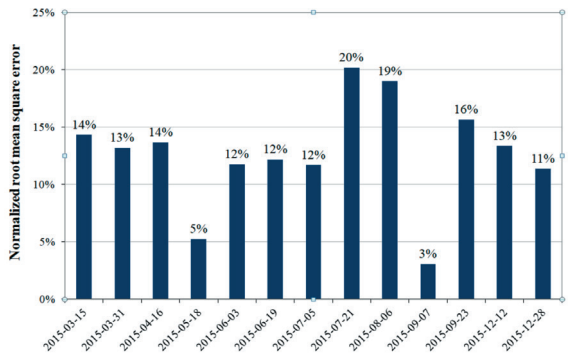

Fig. 6. Estimation root mean square error expressed as percent of the range of Chlorophyll a concentrations measured by ground truth campaign. The x-axis are the dates on which sampling cruises were performed and Landsat 8 imaged the bay

Eutrophication

Figs. 7 and 8 show the daily classification of the bay surface into zones based on the likelihood of eutrophication. The classification has been performed per pixel using the per day method described in the "Detecting eutrophication" section. Different likelihoods of eutrophication were labeled blue, yellow, light red and red for low, possible, probable and certain, respectively. Black areas on the maps represent the land pixels and the white ones represent the areas of sea that could not have been classified because either the sea has been obscured by clouds, their shadows or in one case by smoke from a nearby forest fire.

It should be noted that the areas afflicted by eutrophication (high levels of Chl-*a* concentration) change throughout the year although it is always the inner part of the bay that is most affected. The exceptions to this rule tend to be the southeastern coastal section of Tivat Bay and western coastal section of Herceg Novi Bay.

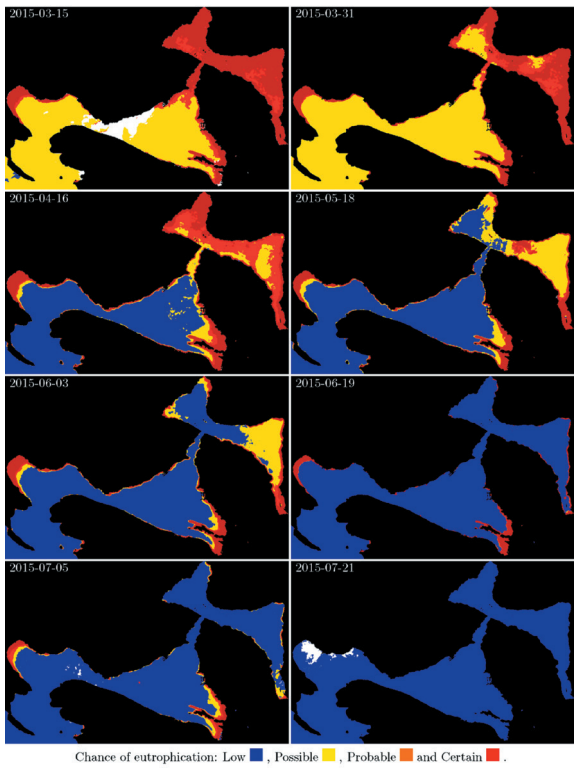

Fig. 7. Eutrophication zones from March to July 2015 based on the daily eutrophication classifier. Classification method has been performed per pixel based on map of Chlorophyll a concentrations estimated from Landsat 8 data

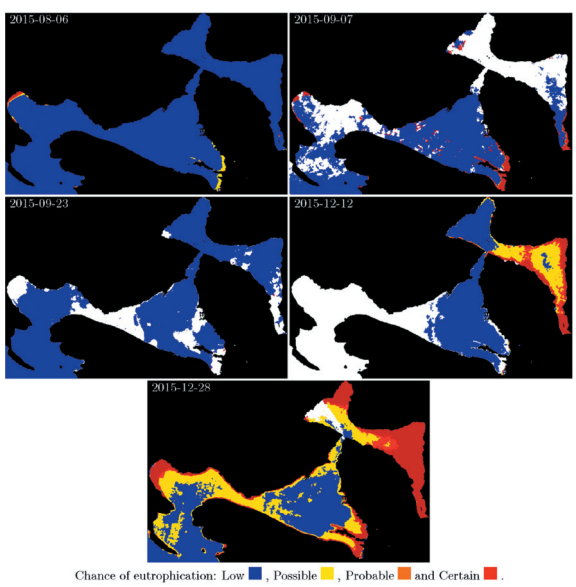

Fig. 8. Eutrophication zones from August to December 2015. Classification method has been performed per pixel based on map of Chlorophyll a concentrations estimated from Landsat 8 data.

Table 2 The performance of the daily eutrophication classifier. The values represent the number of GT samples afflicted ($C_a > 2.21$) or not afflicted ($C_a \leq 2.21$) by eutrophication and assigned by the daily classifiers to the different classes

Class	GT Chl-*a* C_a	
	$C_a \leq 2.21$	$C_a > 2.21$
Low	185	2
Possible	39	7
Probable	3	14
Certain	0	19

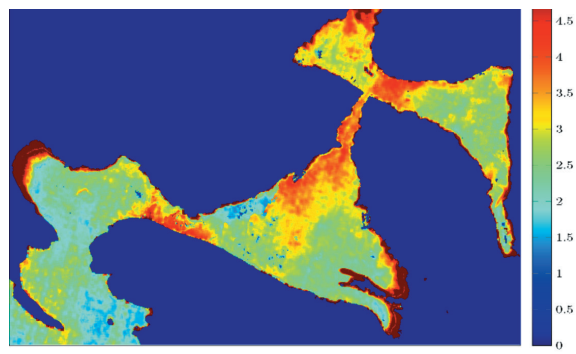

Fig. 9. Yearly eutrophication classification indicator, the ratio of "winter" (non-summer: December-April) maximum to yearly average Chlorophyll a concentration. The ratio was computed per pixel from Chlorophyll a concentrations estimated from Landsat 8 data. Areas with values over 5 can be considered to be under the influence of eutrophication

The result of the yearly classifier is given in Figure 9, which shows a map of yearly eutrophication classification indicator values for 2015. As mentioned previously, yearly eutrophication indicator is the ratio of the maximum (during non-summer months: December-April) to the average Chl-*a* for the entire year. In this case, the ratio was computed per pixel and ratios greater than 5 should indicate the presence of eutrophication.

Figure 10 depicts a comparison of yearly eutrophication indicators, computed from GT (blue solid line) and Chl-*a* values estimated from L8 data (red dashed line). A significant difference between estimated and actual ratio is evident, although estimated ratio does follow the broad trend of the GT values.

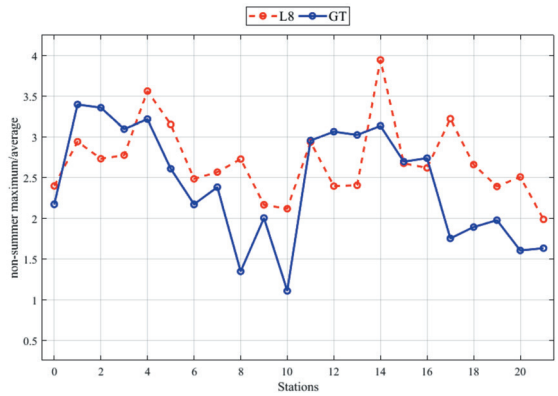

Fig. 10 Comparison of yearly classification indicator (December to April maximum/yearly average) computed from measured (GT-blue solid line) and estimated (L8-red dashed line) Chlorophyll a concentrations.

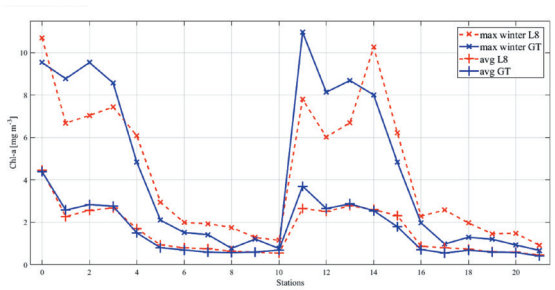

Fig. 11 Comparison of measured (GT-blue solid line) and estimated (L8-red dashed line) "winter" (non-summer: December-April) maxima (marked with x) and average Chlorophyll a concentrations (marked with +) for the entire year

Figure 11 compares the "winter" maxima and averages computed from the L8 and GT data. Only stations 0-21 were used since the data for the rest was only collected during winter however for this indicator concentrations from summer and spring are also needed. Average values are in significantly better agreement than the maxima.

DISCUSSION

This study has shown that L8, with its long revisit time, is especially sensitive to atmospheric conditions. In our case, this has led to months passing without favorable conditions for remote sensing. This vulnerability makes it less than ideal for synoptic monitoring of the ocean water quality with high temporal resolution.

The estimation error of Chl-*a* is mostly low, in comparison to Chl-*a* concentrations (Figs. 3, 5 and 6). The majority of high absolute estimation errors are associated with the inner parts of the bay. However, they are not high compared to actual GT concentrations there. Additionally, the accuracy of the GT campaign is about 10%, so the estimation errors in Figure 5 are to be expected. As expected, both the GT Chl-*a* concentrations and those estimated by the proposed technique show that Chl-*a* is higher during the rainy parts of the year because the rainfall dissolves the limestone mountains surrounding the bay (especially the inner part) which causes higher nutrient inflow (KRIVOKAPIĆ *et al.,* 2009).

The fact that the actual estimation error is lower than the LOO error (0.266 mg m^{-3} and 0.478 mg m^{-3} respectively) is not surprising. After all, for the actual estimation, full datasets were used and not partial ones like for LOO. This additional data point in the actual estimation helped with creating a more suitable model than in the LOO case. While the LOO error is lower than the threshold of 2.21 mg m^{-3} used for eutrophication detection, it is still considerable, which justifies the classification of the bay into zones based on the confidence as shown in "Detecting eutrophication" section.

In (GERACE *et al.,* 2013), it has been theoretically shown that the expected NRMSE of L8 satellite when retrieving Chl-*a* should be around 18%. In practice, (CONCHA & SCHOTT, 2016) reported NRMSE of 13.8%. Figure 6 shows the NRMSE being mostly in range of 10-15% which is consistent with both. Additionally, this is also consistent with the actual measurement error (relative difference) of GT.

The main goal when designing the classifier was the elimination of false positives, i.e. cases when the classifier declares the eutrophication as probable or certain while the actual concentration is less than 2.21 mg m^{-3}. The daily classifier (Table 2) succeeds in that goal since out of 227 GT measurements that are $\leq$ 2.21, only 3 of them, or 1.3%, were false positives. In those three cases, GT Chl-*a* values were 2.08 mg m^{-3}, 2.1 mg m^{-3} and 1.95 mg m^{-3} which is within or close to the average GT measurement error of

0.2, and as such those values might as well have been greater than 2.21 mg m^{-3}. The daily classifier was less successful at eliminating the false negatives (low or possible class when GT Chl-*a* is greater than 2.21 mg m^{-3}). The possible class served its purpose and caught seven out of nine false negatives alerting us that in those areas eutrophication might be happening. Unfortunately, two of the stations with GT Chl-*a* of 2.9 mg m^{-3} and 2.5 mg m^{-3} were classified with low likelihood of eutrophication. Still, failure rate of the proposed technique is only 1.86% (5 out of 269). Taking into consideration many difficulties in the process this is a very low failure rate. Both classifiers identified the northern parts of Risan Bay as the major area afflicted with eutrophication, which is reasonable since it corresponds to a place where the rainwater from the nearby mountains drains into the sea, via Sopot spring, providing a large influx of nutrients after the rain.

The southern tip of Kotor Bay commonly exhibits highest concentrations of Chl-*a* (see Figure 3), and one would therefore assume that it would most likely be undergoing eutrophication. This is confirmed by the daily classificatory results (Figures 7 and 8), yet the yearly indicator values (Figure 9) are in the range of 2-3 (well below the threshold 5) for this area. This is caused by the fact that this classificator tries to find the areas that experience most change in Chl-*a* concentrations during the year. This means it is much more sensitive to the area around Sopot spring which experiences nutrient influxes only after strong rains unlike the southern Kotor Bay which has several potent underwater springs and streams flowing into it providing almost constant influx of nutrients (DRAKULOVIĆ *et al.,* 2017; KRIVOKAPIĆ *et al.,* 2011).

Both shown classifiers seem to be sensitive to shallow sections of the bay, such as the coast of Igalo (north western Herceg-Novi Bay) and south-eastern coast of Tivat Bay, both with depths of less than 10 m. Shallowness probably enables the sunlight reflected from the seafloor to escape the water and make the reflectance detected by L8, a combination of sea-surface and sea floor reflectance.

There are clearly issues with properly estimating the indicator values of the yearly indicator as shown in Figure 10. The Fig. 11 shows that agreement between GT and L8 averages is considerably higher than for the maxima. This is unsurprising, given that averaging is a common strategy to reduce the error of measurement, whereas the maxima retains the original error of estimation. This reliance on a single value (for the maxima) makes the yearly classificator much more error prone than one might expect given the amount of data it uses.

CONCLUSION

The L8 sea surface reflection retrieval algorithm has been provided and an algorithm for retrieval of Chl-*a* from the sea surface reflection using ground truth Chl-*a* measurements has been proposed. Two state-of-eutrophication classifiers have been developed that use estimated Chl-*a* concentrations, one that works with daily datasets and the other that provides a yearly overview.

This research showed that although the Chl-*a* estimation error was not insignificant, it was consistent with (GERACE *et al.,* 2013), and it is possible to use the proposed Chl-*a* estimation and atmospheric correction algorithms to monitor the level of eutrophication in the Boka Kotorska Bay. The daily classifier gives better results whereas the yearly classifier is sensitive to errors introduced by maximum values during computation.

It is shown, that this kind of monitoring using L8 can be highly sensitive to weather conditions since near perfectly cloudless skies are needed and temporal resolution of L8 is low. Another limitation of this technique is the need for ground truth measurements on the day, as close as possible to the time of the satellite overflight.

Still, both classifiers offer the ability of synoptic overview of the state of eutrophication in Boka Kotorska Bay and as such, this monitoring campaign will continue. Sensors (satellite or otherwise) with greater temporal resolution and better atmospheric correction algorithms should be able to help fix some of these issues and reduce the estimation error.

Appendix A: Calculating Sea surface reflectance from L8 images

A.1 Estimating gaseous transmittances

The amount of absorption by the atmospheric gases (O_2, O_3, H_2O etc. (VERMOTE, et al., 2006)) depends on the wavelength of the light, the path through the atmosphere (defined by θ_0 and θ_v, the satellite and sun zenith angles, respectively) and the concentration of the gases.

The gaseous absorption is characterized by the gaseous transmittance t_g. Total gaseous transmittance is a product of the gaseous transmittances of the Sun-sea and sea-sensor paths. Here, we consider only the absorption by water vapor (H_2O) and ozone (O_3) because absorption by other gases in L8 bands 1-5 is negligible. Therefore, t_g can be expressed as:

$$t_g = t_{vH_2O} t_{0H_2O} t_{O_3} \tag{11}$$

where t_{vH_2O} and t_{0H_2O} are the water vapor transmittances for the Sun-sea and sea-sensor paths, respectively, whereas t_{O_3} is the ozone transmittance.

Due to the low absorption of water vapor in L8 bands 1-5 and the fact that θ_v is considerably lower than θ_0 (<10º for most of the area of interest), it can be said that the water vapor transmittance is dominated by the Sun-sea component. Therefore, t_{vH_2O} is approximated to 1. t_{0H_2O} is calculated for each day and each band using the 6S code (VERMOTE, et al., 2006). 6S code is provided with θ_0, the Relative Spectral Responses (RSR) of L8 bands (acquired from (USGS, 2015)) and the Total Perceptible Water (TPW) for considered day. TPW daily maps are provided by the Remote Sensing Systems for each of the satellite instruments they monitor. Temporally and spatially closest value (most often with an offset of 2.7 hours) is selected for TPW.

Ozone transmittance t_{O_3} is calculated using the following expression:

$$t_{O_3}(b) = \exp\left[-\tau_{O_3}(b)\frac{D}{300}\left(\frac{1}{\cos(\theta_0)}+\frac{1}{\cos(\theta_v)}\right)\right], \tag{12}$$

where $\tau_{O_3}(b)$ is the ozone optical thickness for 300 Dobson units (DU) of atmospheric ozone for L8 band b and D is the actual thickness of the ozone layer in DU. $\tau_{O_3}(b)$ has been computed from $\tau_{O_3}(\lambda)$ using weighted mean whose weights are RSR coefficients of the band in question. Values for $\tau_{O_3}(\lambda)$ can be found in (FRANZ, 2015).

A.2 Correcting for Rayleigh scattering

Molecules of atmospheric gases absorb a portion of the light and scatter it, known as Rayleigh scattering, which influences the detected TOA reflectance in two ways. Firstly, due to the scattering, some of the light will be redirected away during both Sun-sea and sea-sensor parts of the path causing less light to be detected by the sensor. This attenuation is characterized by the Rayleigh transmittance t_r. Secondly, due to the scattering, some of the light that would have never hit the sensor, is redirected in the direction of the satellite. Therefore, this causes the atmosphere to be more reflective and this additional reflectance is characterized by the Rayleigh reflectance ρ_r.

Rayleigh reflectance is calculated using expressions from (GORDON, et al., 1988) and (DASH, et al., 2012):

$$\rho_r(b) = \tau_r(b) R(\theta_v, \theta_0, \varphi_v, \varphi_0) \tag{13}$$

$$R(\theta_v, \theta_0, \varphi_v, \varphi_0) = \frac{P_r(\theta_-) + [r(\theta_v) + r(\theta_0)]P_r(\theta_+)}{4\cos(\theta_0)\cos(\theta_v)} \tag{14}$$

where $r(\theta)$ is the Fresnel reflectance for the angle θ, P_r is the Rayleigh scattering phase function, b is band identifier and $\tau_r(b)$ is the optical thickness of the atmosphere in band b.

The term involving θ_- provides the contribution due to photons which are backscattered from the atmosphere without interacting with the sea surface. The terms involving θ_+ account for scattered photons which at some point were specularly reflected from the sea surface. The term $r(\theta_v)$ accounts for the ones scattered before hitting the sea whereas term $r(\theta_0)$ accounts for those that scattered later.

The missing angles $\theta_\pm$, P_r and $r(\theta)$ can be calculated using:

$$P_r(\theta) = 3[1 + \cos(\theta)^2]/4 \quad (15)$$

$$\cos(\theta_\pm) = \pm\cos(\theta_0)\cos(\theta_v) - \sin(\theta_0)\sin(\theta_v)\cos(\phi_v - \phi_0) \quad (16)$$

$$r(\theta) = 0.5\left\{\frac{\sin^2(\theta-\theta_t)}{\sin^2(\theta+\theta_t)} + \frac{\tan^2(\theta-\theta_t)}{\tan^2(\theta+\theta_t)}\right\} \quad (17)$$

$$\frac{\sin(\theta)}{\sin(\theta_t)} = n_w = 1.333 = \quad (18)$$

refractive index of water.

The only remaining unknown is the optical depth of the atmosphere caused by the Rayleigh scattering $\tau_r(b)$,.which depends on the wavelength and atmospheric pressure (P) $\tau_r(\lambda, P) = \tau_r(\lambda)P/101.325$ kPa.

$\tau_r(\lambda)$ has been calculated using the values from tables provided by the OBPG in (FRANZ, 2015). The OBPG values are run through a weighted mean filter whose weights are the RSR of the corresponding band. Since the sampling rates of the data in the OC and RSR tab˙ not same, a linear interpolation of RSR $\rho(NIR)$ is performed using available neighboring RSR values. The RSR for the wavelengths outside of the ranges provided by (USGS, 2015) is considered to be 0.

The Rayleigh transmittance is calculated using relation from (VANHELLEMONT & RUDDICK, 2014):

$$t_r(\lambda) = \exp\left(-\frac{\tau_r(\lambda)}{2\cos\theta}\right), \quad (19)$$

where λ is the wavelength, $\tau_r(\lambda)$ is the optical thickness of the atmosphere caused by Rayleigh effects, and θ is the appropriate zenith angle (θ_0 or θ_v).

A.3 Glint removal

For Sun glint removal we used the method from (HEDLEY *et al.*, 2005) and (KAY *et al.*, 2009), that is based on the idea that there is a linear dependence between the glint in the Near Infra Red (NIR) and other bands. This method includes the following steps:

• Choose a sample of sea pixels whose $\rho_w(NIR)$ can be assumed to be 0, so any reflection in that band is caused solely by the Sun glint. The pixels of the sample should be chosen from all parts of the picture in order to produce a more precise relation. This study uses randomly picked pixels in the open Adriatic Sea.

• Using the reflectance values of these sample pixels and linear regression, determine the linear relation $\rho(B) = k_B\rho(NIR) + n_B$ between reflectances in NIR ($\rho(NIR)$) and visible light bands ($\rho(B)$), where B represents the band in question.

• Determine the minimum NIR reflectance $\rho_{\min}(NIR)$ from the sample.

• Remove glint from each pixel using

$$\rho_{glintless}(B) = \rho(B) - k_B[\rho(NIR) - \rho_{min}(NIR)] \quad (20)$$

where $\rho_{glintless}(B)$, $\rho(B)$ and $\rho(NIR)$ are per pixel values, whereas k_B and $\rho_{min}(NIR)$ are global values for the scene.

ACKNOWLEDGEMENTS

This work has been supported by the Ministry of Science of Montenegro and HERIC project through the BIO-ICT Centre of Excellence (Contract No. 01-1001). Landsat 8 Level 1 scenes courtesy of United States Geological Survey.

REFERENCES

ALLAN, M. G., D.P. HAMILTON, B.J. HICKS, & L. BRABYN. 2011. Landsat remote sensing of chlorophyll a concentrations in central North Island lakes of New Zealand. International Journal of Remote Sensing, 32: 2037-2055.

ANDERSON, D.M., B. REGUERA, G.C. PITCHER & H.O. ENEVOLDSEN. 2010. The IOC International Harmful Algal Bloom Program: History and science impacts. Oceanography, 23(3): 72–85

BARRETT, D. C. & A.E. FRAZIER. 2016. Automated Method for Monitoring Water Quality Using Landsat Imagery. Water, 8: 257 pp.

BELLAFIORE, D., A. GUARNIERI, F. GRILLI, P. PENNA, G. BORTOLUZZI, F. GIGLIO & N. PINARDI. 2011. Study of the hydrodynamical processes in the Boka Kotorska Bay with a finite element model. Dynamics of atmospheres and oceans, 52(1-2), pp. 298-321.

BRANDO, V.E., F. BRAGA, L. ZAGGIA, C. GIARDINO, M. BRESCIANI, E. MATTA, D. BELLAFIORE, C. FERRARIN, F. MAICU, A. BENETAZZO & D. BONALDO. 2015. High-resolution satellite turbidity and sea surface temperature observations of river plume interactions during a significant flood event. Ocean Science, 11(6): p.909.

BRICKER, S.B., B. LONGSTAFF, W. DENNISON, A. JONES, K. BOICOURT, C. WICKS & J. WOERNER. 2007. Effects of Nutrient Enrichment in the Nation's Estuaries: a Decade of Change, National Estuarine Eutrophication Assessment Update. NOAA Coastal Ocean Program Decision Analysis Series No. 26. National Centers for Coastal Ocean Science, Silver Spring, MD. http://ccma.nos.noaa.gov/news/feature/ Eutroupdate.html, pp. 322.

CONCHA, J. A. & J. R. SCHOTT. 2016. Retrieval of color producing agents in Case 2 waters using Landsat 8. Remote Sensing of Environment, 185: 95-107.

DANBARA, T. 2014. Deriving water quality indicators of Lake Tana, Ethiopia, from Landsat 8. Ph.D. Thesis. University of Twente, Netherlands, pp. 68.

DASH, P., N. WALKER, D. MISHRA & S. LADNER. 2012. Atmospheric correction and vicarious calibration of Oceansat-1 Ocean Color Monitor (OCM) data in coastal case 2 waters. Remote Sensing, 4: 1716-1740.

DEGOBBIS D., R. PRESCALI, I. IVANČIĆ, N. SMODLAKA, D. FUKS & S. KVEDER. 2000. Long-term changes in the Northern Adriatic ecosystem related to anthropogenic eutrophication. Int. J. Environ. Pollut. 13: 495-533.

DEVROYE, L., L. GYÖRFI & G. LUGOSI. 2013. A probabilistic theory of pattern recognition (Vol. 31). Springer Science & Business Media, pp. 407-408.

DRAKULOVIĆ, D., S. GVOZDENOVIĆ, D. JOKSIMOVIĆ, M. MANDIĆ & B. PESTORIĆ. 2017. Toxic and Potentially Toxic Phytoplankton in the Mussel and Fish Farms in the Transitional Area of Montenegrin Coast (South-Eastern Adriatic Sea). Turkish Journal of Fisheries and Aquatic Sciences, 17(5): 885-900.

EROS. 2015. (September). LANDSAT 8 (L8) DATA USERS HANDBOOK. Sioux Falls, South Dakota: U.S. Geological Survey (USGS) Landsat Project Science Office at the Earth Resources Observation and Science (EROS) Center. Retrieved from https://landsat.usgs.gov/sites/default/files/documents/Landsat8DataUsersHandbook.pdf

FOCARDI, S., A. SPECCHIULLI, F. SPAGNOLI, F. FIESOLETTI & C. ROSSI. 2009. A combinated approach to investigate the biochemistry and hydrography of a shallow bay in the South Adriatic Sea: the Gulf of Manfredonia (Italy). Environmental monitoring and assessment, 153(1-4): p. 209.

FRANZ, B. 2015. Spectral Response Functions and Bandpass Averaged Quantities. Retrieved February 9, 2015, from http://oceancolor.gsfc.nasa.gov/DOCS/RSR_tables.html

GERACE, A. D., J.R. SCHOTT & R. NEVINS. 2013. Increased potential to monitor water quality in the near-shore environment with Landsat's next-generation satellite. J. of Appl. Remote Sensing, 7: p. 73558.

GORDON, H. R., J.W BROWN & R.H. EVANS. 1988. Exact Rayleigh scattering calculations for use with the Nimbus-7 coastal zone color scanner. Applied optics, 27: 862-871.

HEDLEY, J. D., A.R. HARBORNE & P.J. MUMBY. 2005. Technical note: Simple and robust removal of sun glint for mapping shallow-water benthos. International Journal of Remote Sensing, 26: 2107-2112.

HELLWEGER, F. L., P. SCHLOSSER. U. LALL & J.K. WEISSEL. 2004. Use of satellite imagery for water quality studies in New York Harbor. Estuarine, Coastal and Shelf Science, 61: 437-448.

IRONS, J. R., J. L. DWYER & J. A. BARSI. 2012. The next Landsat satellite: The Landsat data continuity mission. Remote Sensing of Environment, 122: 11-21.

JEFFREY, S.W., R.F. MANTOURA & S.W. WRIGHT.

1997. Phytoplankton pigments in oceanography: guidelines to modern methods. UNESCO Publishing, p. 661.

KAY, S., J.D. HEDLEY & S. LAVENDER. 2009. Sun glint correction of high and low spatial resolution images of aquatic scenes: a review of methods for visible and near-infrared wavelengths. Remote Sensing, 1: 697-730.

KOSTIANOY, A.G., D.M. SOLOVIEV, E.A. KOSTIANAIA, B. ĐUROVIĆ & B. PESTORIĆ. 2016. Satellite Remote Sensing of the Boka Kotorska Bay. In: Joksimović, A., Djurović, M., Semenov, A.V., Zonn, I.S. & Kostianoy, A.G. (Editors). The Boka Kotorska Bay Environment. Springer, Cham. Pa. pp. 495-520.

KOTCHENOVA, S.Y., E.F. VERMOTE, R. MATARRESE & F.J. KLEMM. 2006a. Validation of a vector version of the 6S radiative transfer code for atmospheric correction of satellite data. Applied optics, 45: 6762-6774.

KRIVOKAPIĆ, S., Ž. STANKOVIĆ & N. VUKSANOVIĆ. 2009. Seasonal variations of phytoplankton biomass and environmental conditions in the inner Boka Kotorska Bay (eastern Adriatic Sea). Acta Botanica Croatica, 68: 45-55.

KRIVOKAPIĆ, S., B. PESTORIĆ, S. BOSAK, G. KUŠPILIĆ & C. W. RISER. 2011. Trophic state of Boka Kotorska Bay (South-Eastern Adriatic Sea). Fresenius environmental bulletin, 20(8), pp 1960.

LEPETIĆ, V. 1965. Sastav i sezonska dinamika ihtiobentosa i jestivih avertebrata u bokokotorskom zalivu i mogućnosti njihove eksploatacije. Zavod za biologiju mora, p.100.

MAGAŠ, D. 2002. Natural-geographic characteristics of the Boka Kotorska area as the basis of development. Geoadria, 7: 51-81.

MCCULLOUGH, I.M., C.S. LOFTIN & S.A. SADER. 2012. Combining lake and watershed characteristics with Landsat TM data for remote estimation of regional lake clarity. Remote Sensing of Environment, 123: 109-115.

MÉLIN, F., V. VANTREPOTTE, M. CLERICI, D. D'ALIMONTE, G. ZIBORDI, J.F. BERTHON & E. CANUTI. 2011. Multi-sensor satellite time series of optical properties and chlorophyll-a concentration in the Adriatic Sea. Progress in oceanography, 91(3): 229-244.

MILANOVIC, S. 2007. Hydrogeological characteristics of some deep siphonal springs in Serbia and Montenegro karst. Environmental Geology, 51: 755-759.

NASA. 2015a. MODIS Website - MODIS Specifications. Retrieved March 2015, from http://modis.gsfc.nasa.gov/about/specifications.php

NASA. 2015b. MODIS Website - MODIS Design. Retrieved February 5, 2015, from http://gsfc.nasa.gov/about/design.php

NIXON, S. 2009. Eutrophication and the macroscope. Hydrobiologia 629, 5e19

NEUKERMANS, G., K. RUDDICK, E. BERNARD, D. RAMON, B. NECHAD & P-Y. DESCHAMPS. 2009. Mapping total suspended matter from geostationary satellites: a feasibility study with SEVIRI in the Southern North Sea. Optics Express, 17:14029-14052.

NINČEVIĆ-GLADAN, Ž., M. BUŽANČIĆ, G. KUŠPILIĆ, B. GRBEC, S. MATIJEVIĆ, S. SKEJIĆ, I. MARASOVIĆ & M. MOROVIĆ. 2015. The response of phytoplankton community to anthropogenic pressure gradient in the coastal waters of the eastern Adriatic Sea. Ecological Indicators, 56:106-115.

OLET, E. 2010. Water quality monitoring of Roxo reservoir using Landsat images and In-situ measurements. MS, International Institute for Geo-Information Science and Earth Observation (ITC), ITC, Netherlands, pp. 1-69.

OLMANSON, L.G., S.M. KLOIBER, M.E. BAUER & P.L. BREZONIK. 2001. Image processing protocol for regional assessments of lake water quality. Water Resources Center Technical Report, 14.

OSPAR, 2008. Second OSPAR Integrated Report on the Eutrophication Status of the OSPAR Maritime Area, 2008-372. OSPAR publication, 107 pp.

O'REILLY, J. E.; M.C. O'BRIEN, D.A. SIEGEL, D. TOOLE, D. MENZIES, R.C. SMITH, J.L. MUELLER, B.G. MITCHELL, M. KAHRU, F.P. CHAVEZ, P. STRUTTON, G.E. COTA, S.B. HOOKER, C.R. MCCLAIN, K.L. CARDER, L. HARDING, A. MAGNUSON, D. PHINNEY, G.E. MOORE, J. AIKEN, K.R. ARRIGO, R. LETELIER & M. CULVER. 2000. SeaWiFS Postlaunch Calibration and Validation Analyses, Part 3. NASA Tech. Memo. 2000–206892, 11.

SAVTCHENKO, A., D. OUZOUNOV, S. AHMAD, J. ACKER, G. LEPTOUKH, J. KOZIANA, & D. NICKLESS. 2004. Terra and Aqua MODIS products available from NASA GES DAAC. Advances in Space Research, 34: 710-714.

SCHINDLER, D. W. 2006. Recent advances in the understanding and management of eutrophication. Limnology and Oceanography, 51: 356-363.

SIMBOURA, N., P. PANAYOTIDIS & E. PAPATHANASSIOU. 2005. A synthesis of the biological quality elements for the implementation of the European Water Framework Directive in the Mediterranean ecoregion: the case, of Saronikos Gulf. Ecological Indicators, 5:253-266.

SMODLAKA, N. 1986. Primary production of the organic matter as an indicator of the eutrophication in the northern Adriatic Sea. Science of the total environment, 56: 211-220.

STATISTICAL OFFICE OF MONTENEGRO. 2014. Statistical Yearbook. Podgorica: MONSTAT.

STJEPČEVIĆ, J. & V. ŽUNJIĆ. 1964. Bokokotorski zaliv - fiziografske osobine. Godišnjak geografskog društva SR Crne Gore, pp.75-79.

STRICKLAND, J. D. H. & T. R. PARSONS. 1972. A Practical Handbook of Seawater Analysis. Bulletin Fisheries Research Board of Canada, 167: 1-310.

TETT, P., L. GILPIN, H. SVENDSEN, C. P. ERLANDSSON, U. LARSSON, S. KRATZER, E. FOUILLAND, C. JANZEN, J. Y. LEE, C. GRENZ, A. NEWTON, J.G. FERREIRA, T. FERNANDES & S. SCORY. 2003. Eutrophication and some European waters of restricted exchange. Continental Shelf Research, 23: 1635-1671.

USGS. 2015. Spectral Response of the Operational Land Imager In-Band, Band-Average Relative Spectral Response. Retrieved September 15, 2015, from http://landsat.gsfc.nasa.gov/?p=5779

VOLLENWEIDER, R. A., A. RINALDI & G. MONTANARI. 1992. Eutrophication, structure and dynamics of a marine costal system: Result of ten-year monitoring along the Emilia-Romagna coast (Northwest Adriatic Sea). In: Proceedings of an International Conference "Marine Costal Eutrophication", Bologna, 21-24 March, pp. 63-106.

VANHELLEMONT, Q. & K. RUDDICK. 2014. Turbid wakes associated with offshore wind turbines observed with Landsat 8. Remote Sensing of Environment, 145: 105-115.

VERMOTE, E., D. TANRÉ, J.L. DEUZÉ, M. HERMAN, J.J. MORCRETTE & S.Y. KOTCHENOVA. 2006. Second Simulation of a Satellite Signal in the Solar Spectrum - Vector (6SV). Retrieved May 17, 2016, from http://6s.ltdri.org/files/tutorial/6S_Manual_Part_1.pdf

2005. Phytoplankton pigments in oceanography: guidelines to modern methods. In: Wright, S.W., S.W. Jeffrey & R.F.C. Mantoura (Editors). UNESCO Publishing,

Received: 12 April 2017
Accepted: 23 November 2017

Monitoring eutrofikacije korištenjem satelitske metode Landsat 8 u Bokokotorskom zaljevu

Blažo ĐUROVIĆ*, Igor ĐUROVIĆ, Aleksandar JOKSIMOVIĆ, Vladimir CRNOJEVIĆ, Slobodan ĐUKANOVIĆ i Branka PESTORIĆ

** e-pošta: blazodj@ac.me*

SAŽETAK

Ova studija predlaže metodologiju za nadgledanje koncentracija klorofila-*a* i eutrofičnog stanja u malim zalivima ili u blizini obale. Ova vrsta nadgledanja je zanimljiva jer uobičajena satelitska metodologija, bazirana na MODIS satelitu, nije funkcionalna u ovim oblastima zbog nedovoljne prostorne rezolucije senzora. U ovom radu je predstavljen pristup procjeni koncentracija klorofila-*a* baziran na Landsat 8 satelitskim snimcima i mjerenjima koncentracije obavljenim na određenim lokacijama na dan prelijetanja satelita. Dodatno, dva klasifikatora stanja (dnevni i godišnji) eutrofikacije, koji koriste određene koncentracije, su također prikazani. Preciznost predloženih metoda je procijenjena koristeći „leave-one-out" unakrsnu validaciju, te rezultati pokazuju da je preciznost unutar teoretskih limita metoda baziranih na Ladsat 8 satelitu. Rezultati klasifikatora upoređeni su sa mjerenjima na terenu i pokazuju da je dnevni klasifikator u mogućnosti da klasificira oblast od interesa sa manje of 2% pogreški.

Ključne rıječi: satelitsko nadgledanje, chlorophyll *a*, eutrofikacija, Landsat 8